Molecular Immunology 107 (2019) 44–53

Contents lists available at ScienceDirect

Molecular Immunology

journal homepage: www.elsevier.com/locate/molimm

Granulysin species segregate to different lysosome-related effector vesicles (LREV) and get mobilized by either classical or non-classical degranulation

Marcus Lettau[a,*], Michelle Dietz[a], Katharina Dohmen[a], Matthias Leippe[b], Dieter Kabelitz[a], Ottmar Janssen[a]

[a] Molecular Immunology, Institute of Immunology, Christian-Albrechts-University of Kiel and University Hospital Schleswig-Holstein Campus Kiel, Arnold-Heller-Str. 3, Building 17, D-24105 Kiel, Germany
[b] Comparative Immunobiology, Zoological Institute, Christian-Albrechts-University of Kiel, Olshausenstr. 40, D-24098 Kiel, Germany

ARTICLE INFO

Keywords:
Granulysin
Fas ligand (CD178)
CD107a
Secretory lysosomes
Cytotoxic granules
Lysosome-related effector vesicles
T cells
NK cells

ABSTRACT

Granulysin (GNLY) is a cationic antimicrobial, proinflammatory, and cytotoxic effector protein primarily expressed in human cytotoxic T and NK cells. Its two variants, the 15 kDa precursor and the mature 9 kDa protein processed by proteolysis, act on different microbes or infected and transformed target cells and utilize mechanistically different effector activities. In human peripheral blood lymphocytes of healthy individuals, both forms of GNLY are detected in TCR $\alpha\beta^+$ ($CD4^+$ and $CD8^+$) T cells, TCR $\gamma\delta^+$ T cells, and $CD3^-CD56^+$ NK cells. In general, classical cytotoxic cells (i.e. $CD8^+$ TCR $\alpha\beta^+$ T cells, TCR $\gamma\delta^+$ T cells, and NK cells) contain effector proteins in higher abundance in more cells of the subset as compared to TCR $\alpha\beta^+$ $CD4^+$ T cells. Imaging flow cytometry analyses demonstrate that the subcellular localization and internal pools of 9 kDa and 15 kDa GNLY are virtually non-overlapping. The 9 kDa form is enriched in dense granules that also contain granzymes (Grz) and carry CD107a, whereas 15 kDa GNLY is associated with CD107a-negative lysosome-related effector vesicles. We further demonstrate that 15 kDa GNLY serves as an additional indicator for non-classical, PKC-dependent degranulation while the liberation of granules containing 9 kDa GNLY requires calcium mobilization. Our studies provide a deeper insight into the subcellular localization and release mechanisms of the individual GNLY species. This information will not only be useful for the interpretation of GNLY-related pathophysiologies, but also for the development of therapeutic interventions employing distinct GNLY effector functions for microbial targeting or immunoregulation.

1. Introduction

Granulysin (GNLY) is a cationic cytotoxic effector protein of the saposin-like protein family present in human cytotoxic T lymphocytes (CTL) and Natural Killer (NK) cells (Krensky and Clayberger, 2009). GNLY was found in cytolytic granules with perforin (PRF) and granzymes (Grz) and is released via receptor-mediated degranulation (Stenger et al., 1998). GNLY, however, comes in two flavors with distinct biological properties. The 15 kDa (full length) variant is regarded as a precursor for the short 9 kDa form which is generated by proteolytic processing at both termini from the long form (Pena et al., 1997). It was initially proposed that the 15 kDa GNLY lacks major cytotoxicity against bacterial and mammalian cells, but causes differentiation of monocytes to dendritic cells (Clayberger et al., 2012). However, until recently, the 15 kDa GNLY could not be produced in sufficient quantities and therefore much less was known regarding its potential function except that it had been identified as an important mediator of drug-induced Stevens-Johnson syndrome and as a contributor to graft-versus-host disease (GVHD) and acute transplant rejection (Chung et al., 2008; Nagasawa et al., 2006; Sarwal et al., 2001). Only when the long form was successfully produced as a bioactive recombinant protein, it was reported that 15 kDa GNLY also exerts antimicrobial activity, alters the membrane potential and permeability, but does not disrupt structural integrity of targeted bacteria such as *Pseudomonas*

Abbreviations: BDS, bright detail similarity; CTL, cytotoxic T lymphocyte; GNLY, granulysin; Grz, granzyme; LREV, lysosome-related effector vesicles; mab, monoclonal antibody; pab, polyclonal antibody; PBMC, peripheral blood mononuclear cells; PHA, phytohemagglutinin; PKC, protein kinase C; PRF, perforin; SD, standard deviation; TCR, T-cell receptor

* Corresponding author.
E-mail addresses: Marcus.Lettau@uksh.de (M. Lettau), michelle-dietz@hotmail.com (M. Dietz), dohmenkathi@t-online.de (K. Dohmen), mleippe@zoologie.uni-kiel.de (M. Leippe), Dietrich.Kabelitz@uksh.de (D. Kabelitz), Ottmar.Janssen@uksh.de (O. Janssen).

https://doi.org/10.1016/j.molimm.2018.12.031
Received 20 September 2018; Received in revised form 12 December 2018; Accepted 29 December 2018
Available online 16 January 2019
0161-5890/

aeruginosa (Wei et al., 2016). Similar to several other antimicrobial peptides (AMPs), the antimicrobial activity of 15 kDa GNLY was strongly affected by microenvironment factors such as salts, divalent cations, and changes in pH (Wei et al., 2016).

Previously, a broad antimicrobial and anti-tumor capacity of recombinant 9 kDa GNLY had been shown (Krensky and Clayberger, 2009; Al-Wasaby et al., 2015). The short variant was able to kill bacteria, fungi, yeast, parasites, and tumor cells. As an example, 9 kDa GNLY killed *Mycobacterium tuberculosis* (MTB) by inducing cell surface lesions allowing a PRF-mediated destruction of intracellular MTB (Stenger et al., 1998). Other reported functions of GNLY include its action as a chemoattractant for T lymphocytes, monocytes, and other inflammatory cells, and as a pro-inflammatory modulator of cytokine and chemokine expression (Deng et al., 2005). All in all, GNLY plays an important role not only as a cytotoxic effector protein but also in systemic and local immunomodulation and contributes to several disease-associated pathologies (e.g. in infection, cancer, transplantation, autoimmunity, skin afflictions, and reproductive complications) (Krensky and Clayberger, 2009).

We have shown that the two forms of GNLY segregate to different lysosome-related effector vesicles (LREV) isolated by density gradient centrifugation (Schmidt et al., 2011a). This is in line with a time-dependent processing and the segregation of the two forms of GNLY to different subcellular compartments that had already been proposed when GNLY was identified (Pena et al., 1997). Moreover, it was suggested that 15 kDa GNLY is constitutively secreted by lymphocytes via a non-exocytotic (calcium-independent) pathway, whereas the 9 kDa cytotoxic form is released through calcium-dependent granule exocytosis during target cell killing (Krensky and Clayberger, 2009; Ogawa et al., 2003).

Along this line, we recently demonstrated that individual LREV entities require similarly distinct signals for their mobilization (Lettau et al., 2018). Here, we therefore investigated the abundance, the subcellular localization, and the release of GNLY employing imaging flow cytometry on untransformed human T- and NK-cell populations. We observed that in contrast to the uniform abundance in classical cytotoxic T lymphocytes (CTL, i.e. $CD8^+$TCR $\alpha\beta^+$ T cells or TCR $\gamma\delta^+$ T cells) and almost all $CD3^-CD56^+$ NK cells, only a minor percentage of $CD4^+$ TCR $\alpha\beta^+$ T cells from peripheral blood contain detectable levels of GNLY. This population-specific distribution remains rather stable following primary activation and expansion. Of note, however, when a given cell possesses GNLY, both forms can be detected and their subcellular localization hardly overlaps. Regarding the release of GNLY, we report that the mobilization of the 15 kDa GNLY requires PKC activation only, whereas the release of 9 kDa GNLY is strictly calcium-dependent. These signaling requirements are strictly correlated to those that we described for FasL on the one hand, and for Grzs, PRF, and CD107a on the other hand (Lettau et al., 2018).

We conclude that the two forms of GNLY serve as additional markers for type 1 and type 2 LREV. At the same time, the release of 15 kDa GNLY is an indicator for non-classical (PKC-dependent) degranulation and of the 9 kDa form for classical (calcium-dependent) degranulation. Given the distinct functional properties of 9 kDa and 15 kDa GNLY, the two forms might be separately mobilized by differential activation of $GNLY^+$ cytotoxic effector cells to either induce immunomodulation, tumor cell destruction or target cell perforation and antimicrobial reactivity to resolve infections by intracellular pathogens.

2. Materials and methods

2.1. Cells

Peripheral blood mononuclear cells (PBMC) were isolated by Ficoll (Biocoll, Merck, Darmstadt, Germany) density gradient centrifugation from blood specimen of healthy donors provided by the Institute for Transfusion Medicine of the University Hospital Schleswig-Holstein Campus Kiel. Polyclonal T-cell blasts were generated by incubation of PBMCs (10^6 cells/mL) in RPMI 1640 supplemented with 10% heat-inactivated fetal bovine serum (FBS) and antibiotics (50 U/mL penicillin/50 µg/mL streptomycin, Thermo Fisher Scientific) with 0.5 µg/mL phytohemagglutinin A (PHA, Thermo Fisher Scientific, Waltham, MA, USA). After 3–4 days, dead cells were removed by Ficoll gradient centrifugation and T-cell blasts were expanded in RPMI 1640 medium with rIL-2 (50–100 U/mL, Novartis, Basel, Switzerland). Vδ2 T cells were enriched after initial stimulation of PBMCs with Zoledronate (ZOL, 5 µM, kindly provided by Novartis) and expansion in RPMI 1640 medium with supplements and rIL-2 (50–100 U/mL). For expansion, fresh medium and rIL2 were added every 3–4 days. The phenotype of T-cell lines was periodically analyzed by flow cytometry.

2.2. Ethics statement

All blood donors provided informed consent, and the study was approved by the Institutional Ethics Review Board of the Medical Faculty of the University of Kiel (D485/14).

2.3. Subcellular fractionation

Lysosome-related effector organelles were enriched from expanded human T cells as described previously employing a commercial Lysosome Isolation Kit (Sigma-Aldrich, Taufkirchen, Germany) (Schmidt et al., 2009). Briefly, 4-10^8 T cells were washed with cold PBS and suspended in extraction buffer supplemented with protease inhibitors. Cells were disrupted using a carbide ball cell homogenizer (isobiotec, Heidelberg, Germany). Cell homogenates were centrifuged at 3.400 × *g* for 10 min to pellet nuclei and remaining intact cells. The post-nuclear supernatant was centrifuged at 15.000 × *g* for 20 min and the organelle pellet was adjusted to 19% (v/v) Optiprep® (Sigma) before applying it to a non-ionic, low osmotic discontinuous density gradient with 27, 22.5, 19, 16, 12 and 8% Optiprep® layers. Organelles were separated by ultracentrifugation at 150.000 × *g* for 5 h. The subcellular fractions were collected from the top of the tube, washed and concentrated with HB-Buffer (250 mM sucrose, 10 mM Hepes pH 7.3 and 0.3 mM EDTA) at 15.000 × *g* for 20 min. All ultracentrifugation steps were carried out at 4 °C in Ultra-Clear centrifugation tubes in a swing-out rotor (SW60Ti, Beckman Coulter, Krefeld, Germany).

2.4. Cell stimulation for immunoprecipitation

Zoledronate-expanded ($V\delta2^+$) TCR $\gamma\delta^+$ T cells (14 days of expansion) were adjusted to 2 × 10^6 cells/mL in serum-free X-Vivo medium (Biozym Scientific, Hessisch Oldendorf, Germany) supplemented with antibiotics and rIL-2 (50 U/ml) and 10 mL of the cell suspension were transferred to a 10-cm cell culture dish. TPA (12-*O*-tetradecanoylphorbol-13-acetate, also termed PMA, Merck, final concentration 20 ng/mL) and/or ionomycin (Merck, final concentration 500 ng/mL) were added to stimulate the cells for up to 2 h in the presence or absence of 4 mM EGTA (Merck) and $MgCl_2$ (Merck) at 4 mM. Following stimulation, the cells were washed once with PBS and lysed in a standard NP40 lysis buffer (1% (v/v) Nonidet®P40 (Sigma-Aldrich), 20 mM Tris-buffer, pH 7.4, 150 mM NaCl, 5 mM EDTA) supplemented with protease inhibitors and phosphatase inhibitors (sodium orthovanadate, sodium fluoride, sodium pyrophosphate, phenylmethylsulfonylfluorid, aprotinin, leupeptin and pepstatin A; all from Sigma-Aldrich). The supernatant was centrifuged twice at 3.400 × *g* to remove residual cells and subjected to immunoprecipitation. To this end, NP-40 lysates or supernatants were incubated with 1–2 µg of the respective antibody and protein G-sepharose beads (Sigma-Aldrich) for at least 120 min at 4 °C and subjected to SDS-PAGE after three washing steps in lysis buffer and boiling in reducing sample buffer. The following antibodies were used for immunoprecipitation: anti-GNLY pab (termed “pc” throughout the manuscript, R&D Systems Inc., Minneapolis, MN, USA)

and anti-GNLY mab (clone RF10, MBL International, Woburn, MA, USA).

2.5. Western blot

Proteins were transferred to 0.45 µm nitrocellulose membranes (Protran Premium NC, GE Healthcare) and membranes were routinely blocked with bovine serum albumin (5%, w/v) in Tris-buffered saline containing Tween-20 (TBST). The anti-GNLY pab (R&D Systems), and the anti-FasL mab (clone G247-4, BD Biosciences) were used for detection with respective horseradish-peroxidase conjugated secondary antibodies (GE Healthcare). For re-probing, membranes were incubated in stripping solution (100 mM 2-mercaptoethanol, 2% SDS w/v, 60 mM Tris) for 30 min at 56 °C. ECL reagents (GE Healthcare) were used for chemiluminescent detection using Hyper Film (GE Healthcare). Image analysis for quantitation of band intensities was performed employing GelQuant.NET software provided by biochemlabsolutions.com.

2.6. Immunofluorescent staining

Lymphocytes (1–5 × 10^5 cells) were centrifuged in 96-well V-bottom plates, washed and stained with fluorophore-conjugated monoclonal antibodies directed against surface antigens for 30 min on ice. For staining of intracellular antigens, cells were washed again, fixed, and permeabilized employing the Cytofix/Cytoperm kit (BD-Biosciences) following the manufacturer's instructions. After fixation in 1% paraformaldehyde, the cells were analyzed with an ImageStream X Mark II Imaging flow cytometer. The following antibodies were used for fluorescent labeling of cells: Brilliant Violet 421-conjugated anti-CD4 mab (clone OKT4, BioLegend, San Diego, CA, USA), anti-CD8 mab (clone RPA-T8, BioLegend), anti-CD56 mab (clone HCD56, BioLegend), anti-TCR γδ (clone B1, BioLegend), VioBlue-conjugated anti-TCR Vδ2 (Miltenyi Biotec, Bergisch Gladbach, Germany), PE-conjugated anti-CD107a mab (clone H4 A3, BioLegend), anti-GrzA mab (clone CB9, BioLegend) and anti-GNLY mab (clone DH2, BioLegend), FITC-conjugated anti-CD107a mab (clone H4 A3, BioLegend) unconjugated anti-GNLY mab (clone RF10, MBL International), unconjugated anti-GNLY pab (RD Systems, Minneapolis, MN, USA). Alexa Fluor 555-conjugated donkey anti-mouse pab, Alexa–Fluor 647 conjugated donkey anti-mouse and donkey anti-goat pab (all from Thermo Fisher Scientific) served as secondary antibodies. In experiments requiring anti-mouse secondary reagents, CD56 and the γδ TCR were stained in a last step with fluorophore-conjugated antibodies. PE-conjugated IgG1 (clone 1F8, Immunotools, Friesoythe, Germany) and FITC-conjugated IgG1 (clone 203, Immunotools) served as isotype controls.

2.7. Imaging flow cytometry

The ImageStream X Mark II (Merck Millipore, Burlington, MA, USA) one camera system with 351, 488, 562, 658 and 732 nm lasers was used for imaging flow cytometry. The system was calibrated using SpeedBeads (Amnis, Seattle, WA) prior to use and at least 10.000 events with an area > 15 $µm^2$ based on brightfield images per experimental or isotype control samples were acquired. Moreover, 1.000 events of single stained compensation control samples gated on appropriate signal size were acquired with both the bright field channel and the 732 nm laser turned off. Images were acquired at 60fold magnification with the following parameters: Brilliant Violet 421 in channel 1, FITC and Alexa Fluor 488 in channel 2, PE and Alexa Fluor 555 in channel 3, Far red fixable dye, Alexa Fluor 647 and APC in channel 5 and bright field in channel 6. The integrated software INSPIRE (Merck Millipore) was used for data collection as raw image files. Raw image files of a respective staining and the corresponding isotype or unstained control files were merged. Single color controls were used to calculate a spectral crosstalk matrix that was applied to each raw image file for spectral compensations in the detection channels. Analysis was performed on the compensated image files using IDEAS (Merck Millipore) image analysis software. The bright field gradient root mean square (RMS) feature was used to gate on focused cells. Bright field area versus aspect ratio features were plotted and used to gate on single cells. Dead cells were excluded from the analysis based on the fluorescence intensity in channel 5. Cells with saturated pixels were excluded from the analysis by plotting the histogram for the Saturation Count feature (number of saturated pixels in each cell) and gating on cells with a saturation count of 0. Analyte-positive cells were discriminated based on isotype and/or unstained controls. The Bright Detail Similarity R3 feature was used to quantify the degree of co-localization in double positive cells only.

2.8. Statistical analysis

The paired, two-tailed Student's *t*-test was performed. Statistical significance was set at $p < 0.05$ and displayed as ** for $p < 0.01$ and * for $p < 0.05$.

3. Results

3.1. Differential distribution of granulysin in $CD4^+$ and $CD8^+$ lymphocyte subsets

In cytotoxic T cells and NK cells, the effector protein GNLY comes in two flavors which are supposedly associated with distinct subcellular storage/effector compartments. In order to investigate the overall GNLY expression, the subcellular localization and the mobilization of individual GNLY species, we first analyzed unstimulated peripheral blood mononuclear cells (PBMC) and polyclonally expanded PHA blasts at days 7 and 14 of expansion by imaging flow cytometry. The gate was set on focused, single, viable cells and we initially analyzed the presence of GNLY in $CD4^+$ and $CD8^+$ cells within the whole blast population. Among the $CD8^+$ cells, we observed two subpopulations which differed in CD8 levels and in GNLY expression. A counterstaining for the NK cell marker CD56 in a separate experiment revealed that only 10–15% of the larger population of $CD8^{high}$ cells but 70% of the smaller subset of $CD8^{low}$ cells are $CD56^+$ (not shown). In individual experiments, we noted that the percentage of these three individual subsets differed between donors not only at the onset of the experiment, but also following expansion (indicated by respective SDs in Fig. 1A). Consistent for all donors, in resting (d0) cells, between 0.5 and 2% of $CD4^+$ and between 2.9 and 8.7% of $CD8^{high}$ cells contained detectable levels of GNLY (Fig. 1B). By contrast, we noted that of the small population of $CD8^{low}$ (NK) cells, between 53.8% and 72.4% were GNLY-positive. This differential distribution was maintained during expansion after PHA stimulation. At day 14, the portion of $GNLY^+$ $CD4^+$ cells remained in the range of only 1%, whereas that of $GNLY^+$ $CD8^{high}$ cells increased to 14.5% and the highest percentage of $GNLY^+$ cells was still detected in the $CD8^{low}$ population (35.5%). In sum, these data reveal that in $CD8^{high}$ CTL, granulysin expression tends to increase upon activation although differences were not significant among three donors. In freshly isolated $CD8^{low}$ NK cells, granules are already formed and granulysin expression rather decreases upon expansion.

3.2. Granulysin association with intracellular vesicles

Since only a few $CD4^+$ T cells contain GNLY, we focused for the following analysis on $CD8^+$ cells representing the classical cytotoxic T-cell and NK-cell populations. To investigate the subcellular localization of GNLY, we used CD107a (Lamp-1) as a lysosomal marker to stain intracellular vesicles. The ImageStream analyses revealed an evident association of GNLY with CD107a-positive vesicles in both $CD8^{high}$ and $CD8^{low}$ cells. The Bright Detail Similarity (BDS) scores calculated for $GNLY^+$ cells in each subset serve as a measure for co-localization. A geometric mean value above 2 is regarded as a proof for (partial) co-localization. In the representative experiment depicted in Fig. 2A and B,

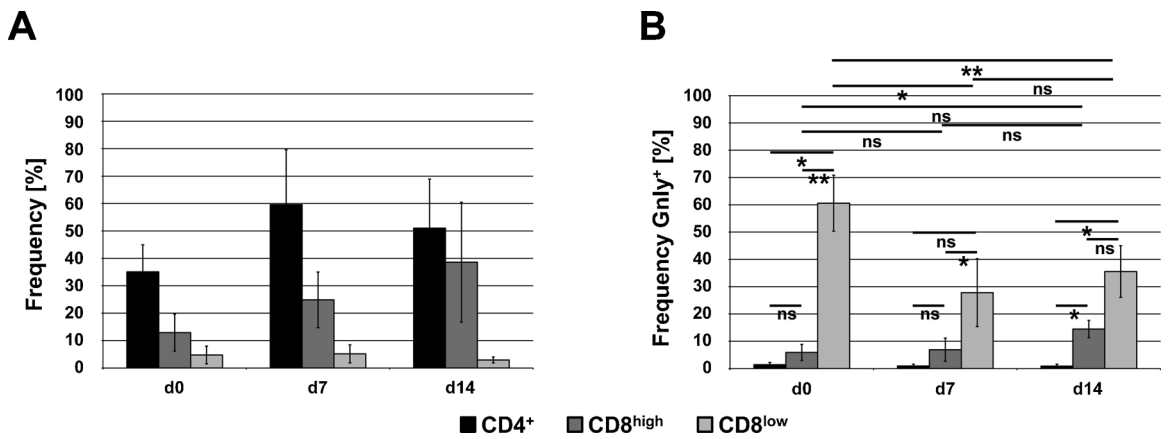

Fig. 1. Differential distribution of granulysin in $CD4^+$, $CD8^{low}$ and $CD8^{high}$ cells. PBMCs (d0) and T-cell blasts activated with PHA for 7 and 14 days (d7, d14) were stained with a LIVE/DEAD™ Fixable Far Red Dead Cell Stain, fixed, permeabilized and stained with Brilliant Violet 421-conjugated anti-CD4 mab (clone OKT4) or anti-CD8 mab (clone RPA-T8), and PE-conjugated anti-GNLY mab (clone DH2) or appropriate isotype controls. A total of 10.000 cells were acquired with an ImageStream Mark II imaging flow cytometer. Only focused, single, viable cells were considered for further analyses. (A) Bars display the frequency of $CD4^+$ (black bars), $CD8^{high}$ (dark grey bars) and $CD8^{low}$ (light grey bars) cells among focused, single, viable PBMCs (d0) and in T-cell blasts after 7 and 14 days of expansion. (B) Bars display the percentage of $CD4^+$ (black bars), $CD8^{high}$ (dark grey bars) and $CD8^{low}$ (light grey bars) cells expressing GNLY. Data are displayed as mean values +/- standard deviation of cells derived from three different donors. Statistical significance between different populations and expansion times is displayed as * for $p < 0.05$ and ** for $p < 0.01$ (Student's *t*-test; ns: not significant).

geometric mean BDS values for $CD8^{high}$ and $CD8^{low}$ cells are comparable at 2.476 and 2.508, respectively. The percentage of cells with a BDS > 2 was in the same range for $CD8^{high}$ (82.4%) and $CD8^{low}$ (83.3%) cells. Similar results were obtained in separate analyses from three different donors (Fig. 2C and D).

3.3. Granulysin species segregate to different subcellular compartments

On Western blots of individual subcellular compartments from human T-cell blasts, we had previously noted that the individual 9 kDa and 15 kDa forms of GNLY might segregate to distinct LREV (Schmidt et al., 2011a, 2009). We followed this observation and analyzed the

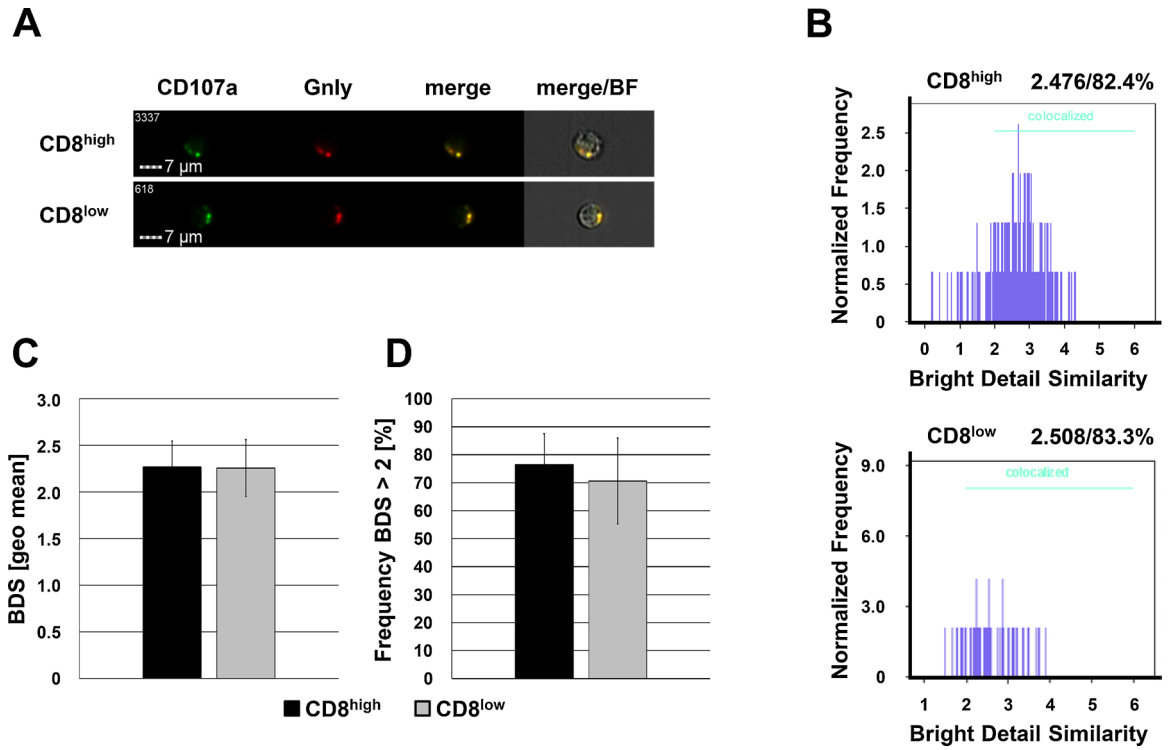

Fig. 2. Comparable vesicular expression of granulysin in $CD8^{low}$ and $CD8^{high}$ cells. PHA-activated T-cell blasts (day 15) were stained with a LIVE/DEAD™ Fixable Far Red Dead Cell Stain, fixed, permeabilized and stained with Brilliant Violet 421-conjugated anti-CD8 mab (clone RPA-T8), FITC-conjugated anti-CD107a mab (clone H4A3) and PE-conjugated anti-GNLY mab (clone DH2) or appropriate isotype controls. A total of 10.000 cells were acquired with an ImageStream Mark II imaging flow cytometer. Only focused, single, viable $CD8^+$ cells were considered for further analyses. (A) Representative images of $CD107a^+/GNLY^+$ double-positive cells are shown. Scale bars represent 7 µm. (B) The BDS R3 feature was used to quantify the degree of co-localization. Representative histograms displaying the BDS score are shown for $CD8^{high}$ and $CD8^{low}$ cells, respectively, with indication of the geometric mean value of the BDS score and the percentage of cells displaying a BDS score > 2. (C) Geometric mean value of the BDS score and (D) the percentage of $CD8^{high}$ (black bars) and $CD8^{low}$ (grey bars) cells displaying a BDS score > 2. Data are displayed as mean values +/- standard deviation of T-cell blasts derived from three different donors.

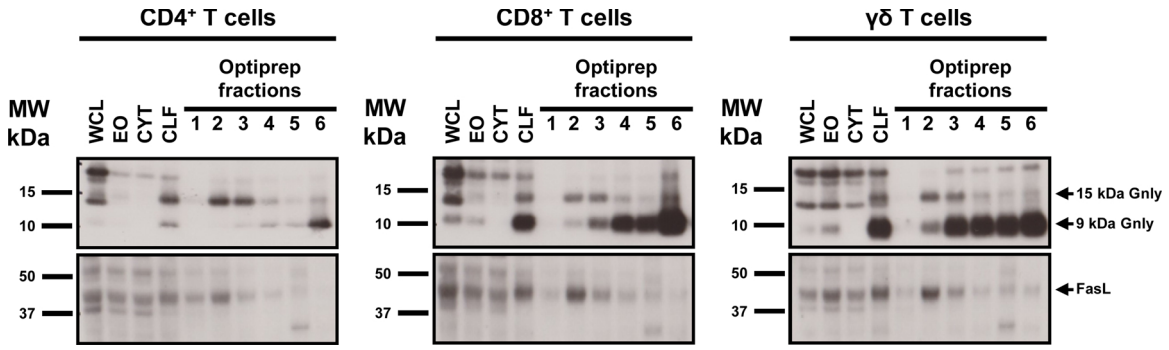

Fig. 3. Differential distribution of granulysin and FasL in individual LREV. CD4$^+$ and CD8$^+$ T cells were MACS purified, PHA-stimulated and expanded in the presence of rIL-2. TCR γδ$^+$ T cells were enriched by zoledronate-stimulation from PBMC and expansion in rIL-2-containing medium. After two weeks of expansion, the cells were harvested and homogenized using a carbide ball homogenizer. Organelles were enriched as described and aliquots of whole cell lysates (WCL), enriched organelles (EO), cytosol (CYT), and crude lysosomal fraction (CLF) were kept for the Western blot analysis. The CLF was then loaded on a discontinuous Optiprep gradient. Three µg total protein of the indicated controls and individual fractions obtained after ultracentrifugation were loaded per lane. The Western blot was stained with a polyclonal anti-GNLY antibody (anti-GNLY (pc), upper panels) and visualized with a HRP-conjugated secondary antibody. The gels were stripped and further stained for FasL (mouse mab G247/4 from BD Biosciences, lower panel) using a respective anti-mouse IgG secondary antibody.

distribution of GNLY in enriched organelles from MACS-sorted CD4$^+$ or CD8$^+$ T-cell blasts and zoledronate-stimulated (thus Vδ2$^+$) TCRγδ$^+$ T cells after two weeks of expansion. After mild homogenization, organelles were enriched by differential centrifugation and subsequent ultracentrifugation on a discontinuous optiprep/iodixanol gradient. Confirming our previous notion for unseparated PHA blasts, in all tested subpopulations the unprocessed 15 kDa GNLY is detected in less dense LREV (fractions 2–3 of the respective gradients), whereas the processed 9 kDa form is much more abundant in the denser vesicles, and especially in those of fraction 6 (Fig. 3, upper panels). As a control for less dense LREV, we also probed the blot for FasL (CD178) which we defined as a marker for this entity in previous studies (Lettau et al., 2018; Schmidt et al., 2011a, b). In agreement with these earlier results, we find the strongest signal for FasL in less dense LREV in fraction 2. We are fully aware that levels of GNLY content in individual subpopulations might not be deduced from these blots, however, since equal amounts of protein were loaded for all cell types, the relative abundance of effector proteins present in whole cell lysates and control samples, especially the crude lysosomal fraction (CLF), and also in fractionated vesicles from individual cell populations appeared to differ substantially. As already depicted in Fig. 1 the pool of stimulated CD4$^+$ T cells contains less GNLY than CD8$^+$ T cells (here comprising CD8^{high} and CD8^{low} cells) and TCR γδ$^+$ T cells.

3.4. Intracellular localization of 9 and 15 kDa granulysin

We next employed imaging flow cytometry to verify and statistically proof not only that both forms of GNLY are expressed in individual cells but that the 9 kDa and 15 kDa variant segregate to different subcellular compartments. These analyses were performed with unstimulated PBMC gated on CD56$^+$ NK cells and with expanded γδ T cells since these lymphocyte subpopulations revealed the most pronounced GNLY abundance. In order to differentiate between the two forms of GNLY, we made use of the differential binding properties of two established GNLY detection reagents. The monoclonal antibody (mab) RF10 exclusively binds to the full length 15 kDa variant, whereas the employed polyclonal antibody (pab) pc almost exclusively recognizes the 9 kDa form in PFA-fixed samples (Clayberger et al., 2012). Of the analyzed TCR γδ$^+$ cells, on average 46% were stained positive for the 15 kDa variant with mab RF10 and 31% for the 9 kDa variant with the pab (pc) (Fig. 4A). Of the CD56$^+$ cells, 79% and 64% store the 15 kDa and 9 kDa GNLY form, respectively (Fig. 4B). Moreover, both antibodies stain their respective target in granular structures in individual cells (Fig. 4C/D). Although we frequently observed a higher frequency of cells expressing the 15 kDa variant compared to expression of the 9 kDa variant, those sporadic differences were not significant. Interestingly, in both CD56$^+$ NK cells and TCR γδ$^+$ T cells, 15 kDa GNLY hardly co-localizes with the effector granule marker CD107a whereas the 9 kDa form apparently localizes to CD107a$^+$ granules (Fig. 4C/D). In addition, in TCR γδ$^+$ T cells, the 9 kDa but not the 15 kDa form co-localizes with the cytotoxic effector protease GrzA (Fig. 4C).

Consequently, the bright detail similarity score for the co-localization of 15 kDa GNLY with CD107a (0.85) and GrzA (1.11) is rather low in TCR γδ$^+$ T cells (Fig. 5A) and with CD107a also in CD56$^+$ NK cells (0.83; Fig. 5C). Moreover, only 1.2% (CD107a) and 7.2% (GrzA) of GNLY$^+$/TCR γδ$^+$ cells (Fig. 5B) and 1.4% of GNLY$^+$/CD56$^+$ cells (Fig. 5D) display a BDS score > 2. In contrast, the bright detail similarity score for the co-localization of 9 kDa GNLY with CD107a (1.7 for both TCR γδ$^+$ and CD56$^+$) and with GrzA (1.8) is significantly higher with 38.8% (CD107a) and 43.1% (GrzA) of TCR γδ$^+$ cells and 39.7% of CD56$^+$ cells displaying a BDS score > 2. Consequently, the 15 and 9 kDa forms of GNLY segregate to individual granular structures resulting in a lower BDS score of 1.2 in the case of TCR γδ$^+$ cells and 1.1 in CD56$^+$ cells. Along this line, only 7.7% of TCR γδ$^+$ cells and 7.5% of CD56$^+$ cells display a BDS score > 2. Of note, similar results were also obtained in unstimulated PBMC gated on CD4$^+$, CD8$^+$, and TCR Vδ2$^+$ cells (Suppl. Fig. 1).

3.5. Differential activation-induced release of 9 or 15 kDa granulysin

We recently reported that individual LREV employ different molecular routes for their mobilization and release that go along with the definition of non-classical and classical degranulation (Lettau et al., 2018). We thus employed the two different detection reagents to analyze the signal requirements for the release of the two forms of GNLY. As mentioned, mab RF10 exclusively binds to the full length 15 kDa variant (see also Western blot of RF10 immunoprecipitation from whole cell lysate in Fig. 6), whereas the pab (pc) apparently is able to immunoprecipitate both forms with a preference for the processed 9 kDa form (see IP from whole cell lysate with anti-GNLY (pc)). The polyclonal anti-GNLY antibody (pc) was therefore also used as a primary antibody for GNLY detection on the Western blot. Following this strategy, we were able to determine which form of GNLY is secreted into the culture supernatant upon stimulation with either phorbol ester and/or calcium ionophore, mimicking either calcium-independent non-classical degranulation by PKC-induction or calcium-dependent classical degranulation. As exemplarily shown in Fig. 6A/B for TCR γδ$^+$ cells, we precipitated GNLY with the polyclonal anti-GNLY (pc) antibody from culture supernatants of unstimulated or TPA- and TPA/ionomycin-stimulated cells. TPA-activation results in an increased and

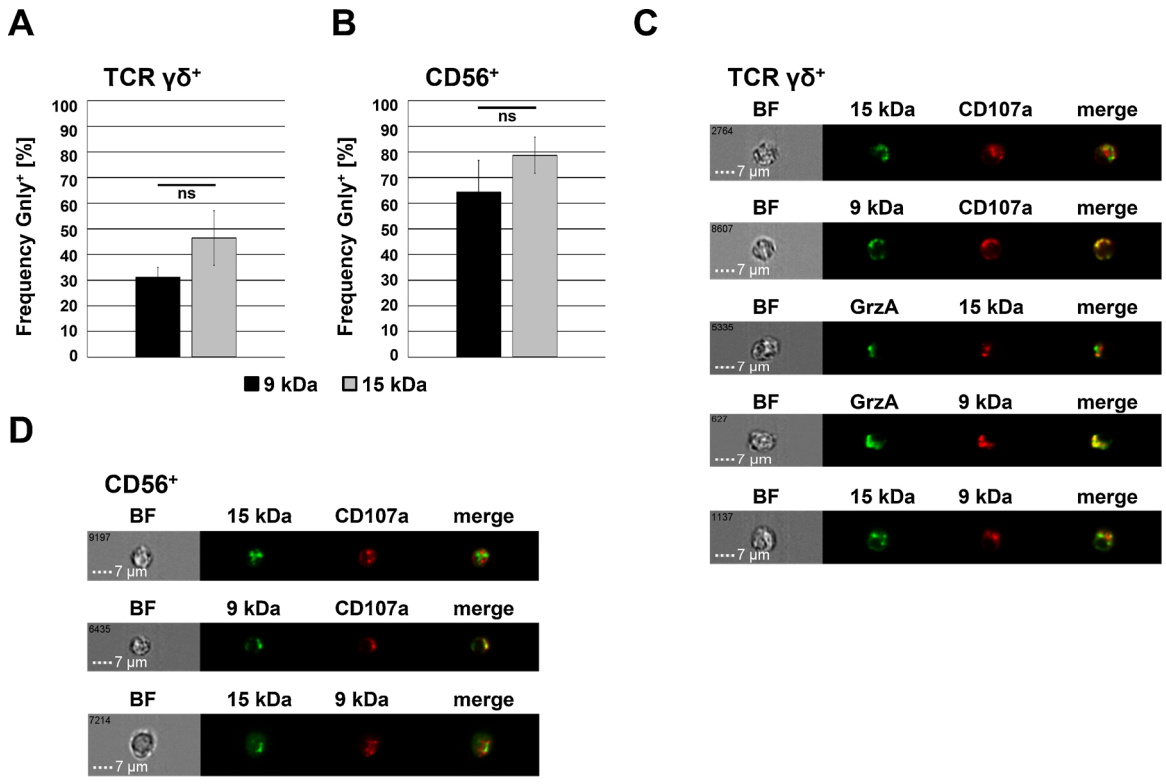

Fig. 4. 9 kDa and 15 kDa granulysin segregate to different intracellular storage compartments. PBMC were either stimulated with Zoledronate to activate TCR $\gamma\delta^+$ T cells and expanded for 14 days in the presence of rIL-2 (A/C) or directly used for analysis (B/D). Cells were fixed, permeabilized and stained with anti-GNLY mab RF10 and/or a polyclonal anti-GNLY pab (pc) and appropriate Alexa Fluor 555- or Alexa Fluor 647-conjugated secondary antibodies. After washing, cells were additionally stained or not with a PE-conjugated anti-CD107a mab (clone H4A3) or an anti-GrzA mab (clone CB9) and a Brilliant Violet 421-conjugated anti-TCR γδ (clone B1; A/C) or an anti-CD56 (clone HCD56; B/D) mab. A total of 10.000 cells were acquired with an ImageStream Mark II imaging flow cytometer. Only focused, single, TCR $\gamma\delta^+$ (A/C) or $CD56^+$ (B/D) cells were considered for further analyses. (A/B) Bars display the percentage of 9 kDa $GNLY^+$ (black bars) and 15 kDa $GNLY^+$ (grey bars) TCR $\gamma\delta^+$ (A) or $CD56^+$ (B) cells. Data are displayed as mean values +/- standard deviation of cells derived from three different donors. (C/D) Representative images of 15 kDa $GNLY^+/CD107a^+$, 9 kDa $GNLY^+/CD107a^+$, 15 kDa $GNLY^+/GrzA^+$, 9 kDa $GNLY^+/GrzA^+$ and 15 kDa $GNLY^+$/9 kDa $GNLY^+$ double-positive TCR $\gamma\delta^+$ (C) or $CD56^+$ (D) cells are shown. Scale bars represent 7 µm.

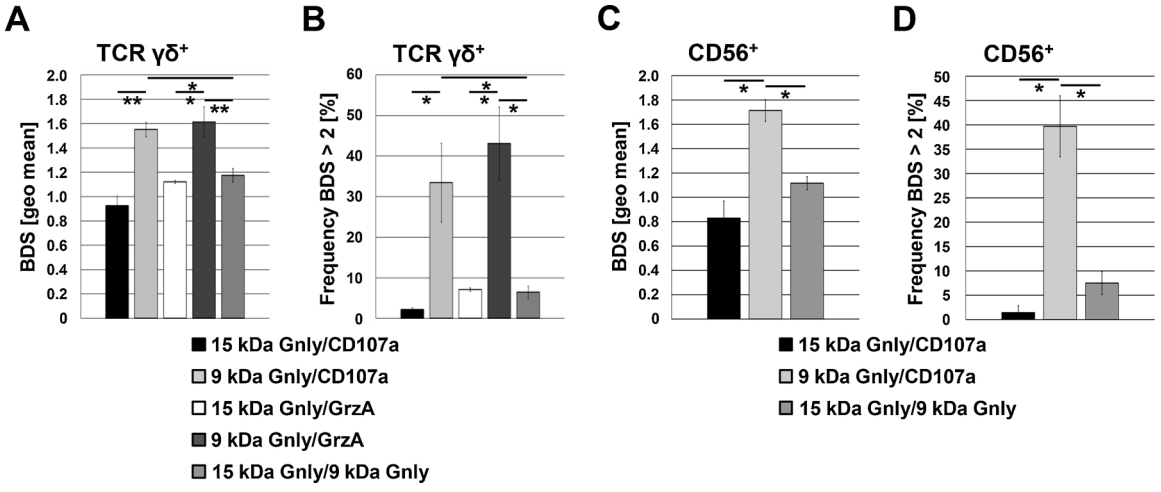

Fig. 5. Segregation of 9 kDa and 15 kDa granulysin to different intracellular storage compartments. PBMC were either stimulated with Zoledronate to activate TCR $\gamma\delta^+$ T cells and expanded for 14 days in the presence of rIL-2 (A/B) or directly used for analysis (C/D). Cells were fixed, permeabilized, and stained with anti-GNLY mab RF10 and/or a polyclonal anti-GNLY pab (pc) and appropriate Alexa Fluor 555- or Alexa Fluor 647-conjugated secondary antibodies. After washing, cells were additionally stained or not with a PE-conjugated anti-CD107a mab (clone H4A3) or an anti-GrzA mab (clone CB9) and a Brilliant Violet 421-conjugated anti-TCR γδ (clone B1; A/B) or an anti-CD56 mab (clone HCD56; C/D). A total of 10.000 cells were acquired with an ImageStream Mark II imaging flow cytometer. Only focused, single, TCR $\gamma\delta^+$ (A/B) or $CD56^+$ (C/D) cells were considered for further analyses. (A/C) Bars display the geometric mean value of the BDS score and (B/D) the percentage of cells displaying a BDS score > 2. Data are displayed as mean values +/- standard deviation of cells derived from three different donors. Statistical significance is displayed as * for $p < 0.05$ and ** for $p < 0.01$ (Student's *t*-test).

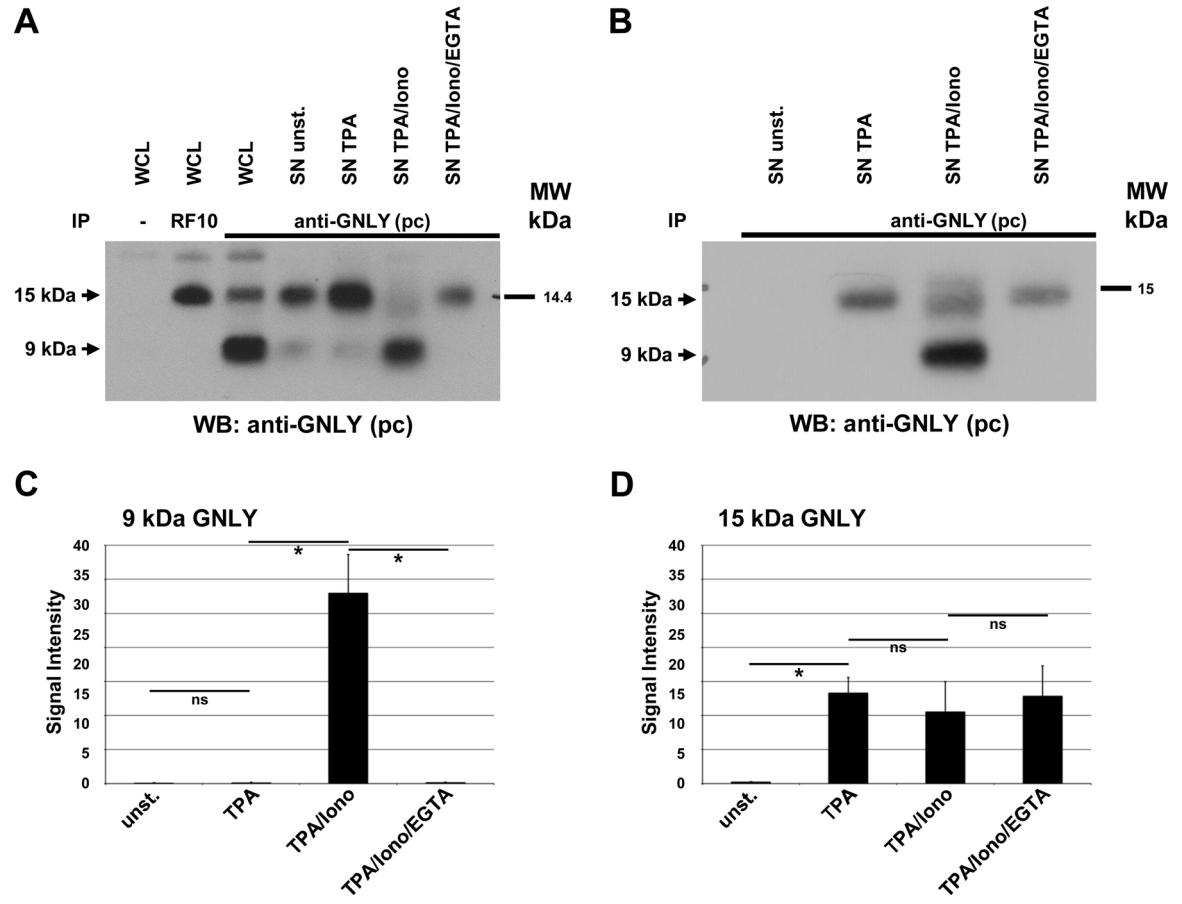

Fig. 6. Different forms of granulysin are separately released upon T cell stimulation. PBMC were stimulated with Zoledronate to activate TCR $\gamma\delta^+$ T cells. After expansion for 14 days in the presence of rIL-2, the cells were transferred to 10-cm culture dishes and stimulated or not for two hours with TPA and/or Ionomycin with or without EGTA. (A) Control precipitations were performed from NP40 lysates (whole cell lysate, WCL) of unstimulated cells with protein G beads alone, with mab RF10, or the polyclonal anti-GNLY antibody (pc). (A/B) Precipitations from supernatants (SN) of unstimulated or stimulated cells were performed with anti-GNLY only (pc). The blot was stained with the anti-GNLY (pc) to detect both forms of GNLY as detailed in the results section. (C/D) Densitometric analysis of three independent experiments as depicted in (B) for (C) 9 kDa GNLY and (D) 15 kDa GNLY. Data are displayed as mean values +/- standard deviation. Statistical significance between different stimulation conditions is displayed as * for $p < 0.05$ (Student's *t*-test; ns: not significant).

selective release of the 15 kDa variant into the culture supernatant, whereas TPA in combination with ionomycin induces a prominent (Ca^{2+}-dependent) release of the 9 kDa form. Importantly, this Ca^{2+}-dependent release triggered by TPA in combination with ionomycin can be completely abrogated by Ca^{2+}-chelation using EGTA. Notably, both the TPA/Ionomycin-mediated release of 9 kDa GNLY and its inhibition by EGTA (Fig. 6C) as well as the TPA-mediated release of 15 kDa Gnly (Fig. 6D) are highly reproducible.

4. Discussion

Cytotoxic T cells and Natural Killer cells share a common arsenal of effector proteins to eliminate virus-infected or transformed tumor cells and to contribute to host defense against intracellular pathogens. It is widely accepted that cytotoxic T cells (CTL) develop their cytolytic effector potential and build storage vesicles in a regulated manner upon activation, whereas NK cells are constitutively equipped with respective effector granules. Only upon (differential) recognition of respective target cells, individual subtypes of innate and adaptive killer cells mobilize different lysosome-related effector vesicles (LREV) to the cytotoxic immunological synapse (Lettau et al., 2015). These granules contain a variety of different effector proteins including death factors, pore-forming proteins, and proteases. In essence, death ligands of the TNF superfamily such as FasL and TRAIL are brought to the cell membrane to trigger death-receptor mediated apoptosis while soluble factors are released into the synapse to penetrate the target cell and allow the entry of other effectors into its cytosol (Lettau et al., 2015; Martinez-Lostao et al., 2015).

The so far best studied pore-forming protein within effector granules is PRF, which at sublytic concentrations opens the target-cell membrane for serine proteases such as Grzs which are presumably released concomitantly from the same vesicular entity. Grzs subsequently destroy the target cell, e.g. by initiating caspase-dependent or -independent cell death. Interestingly, human but not rodent T and NK cells also release GNLY as an additional membrane-attacking component (Krensky and Clayberger, 2009). GNLY structurally belongs to the family of saposin-like proteins that fulfill different functions but have in common that they interact with membrane lipids (Anderson et al., 2003; Kolter et al., 2005). Other members of this protein family with antimicrobial and cytotoxic activity are NK-lysin of porcine lymphocytes (Liepinsh et al., 1997) and amoebapores from pathogenic amoebae (Hecht et al., 2004). Walch and colleagues showed that GNLY especially acts in a cholesterol-poor membrane environment as found in intracellular parasites embedding the core components of the electron transport chain. They proposed that PRF enables the entrance of Grzs and GNLY into the infected cell where GNLY in turn introduces Grzs into the intracellular bacteria to cause irreversible damage of the pathogen (Dotiwala et al., 2016; Walch et al., 2014). Interestingly, it has only recently been shown that different subsets of T and NK cells are equipped with individual combinations of the key effectors GrzB, PRF, and GNLY (Dotiwala et al.,

2016). Moreover, for instance in leprosy patients such mono-, di- or tri-cytotoxic T lymphocytes substantially differ in their antimicrobial defense capacity against *Mycobacterium leprae* (Balin et al., 2018).

Although the role of GNLY as a cytotoxic weapon for antimicrobial defense is well-accepted, the molecular peculiarities of this effector protein left a number of open questions regarding its intracellular processing, storage, and mobilization. The mature 9 kDa GNLY is released from a 15 kDa precursor by proteolytic cleavage at both ends of the molecule (Krensky and Clayberger, 2009). It was noted earlier that the two GNLY species are found in different subcellular localizations what may also be reflected by different release mechanisms. It was thus proposed that the 15 kDa form is constitutively secreted whereas the 9 kDa form is released by receptor-mediated granule exocytosis (Krensky and Clayberger, 2009). Since the two forms exert mechanistically different antimicrobial or cytotoxic features, GNLY has meanwhile developed as an important diagnostic and prognostic factor and as a therapeutic target for numerous diseases including infection, cancer, transplantation, or autoimmunity, and for certain diseases of the skin and the reproductive tract. Moreover, recombinant GNLY or synthetic derivatives thereof are being developed as immunomodulatory or antimicrobial agents and as a new class of antibiotics to fight tuberculosis (Che et al., 2016; Kita et al., 2013).

Our present ImageStream analyses confirm that GNLY is present in all T-cell subsets and in NK cells (Fig. 1). However, only a small percentage of freshly isolated or activated $CD4^+$ T cells is $GNLY^+$. As expected, classical cytotoxic T cells expressing high amounts of $CD8^+$ contain higher amounts of GNLY in more cells of the cell population than $CD4^+$ T cells. Notably, even after activation and expansion the percentage of $CD8^{+high}$ $GNLY^+$ T cells is still in the range of 10–20% only, supporting the recent finding that not all CTL develop to fully equipped tri-cytotoxic CTL (Balin et al., 2018). By contrast, in CTL the activation-dependent maturation of LREV is reflected by an increase in synthesis of GrzA and GrzB, and PRF (not shown). During the initial analyses of T cells, we noticed that one could discriminate two subpopulations of $CD8^+$ T cells that differed in CD8 expression and GNLY content. Of the small population of $CD8^{low}$ cells, 60% were constitutively $GNLY^+$ (Fig. 1B). Of note, $CD8^{low}$ represent a subset of NK cells as revealed by counterstaining for CD56 in separate experiments. As shown in Figs. 2 and 4, GNLY was detected in all tested cell subpopulations in intracellular granular structures that were also positive for the lysosomal marker CD107a (LAMP-1). Since classical degranulation is accompanied by CD107a mobilization to the cell surface, this protein is also the most common marker to assess the cytolytic activity of T and NK cells (Alter et al., 2004; Betts et al., 2003).

We previously described two distinct species of lysosome-related secretory vesicles (LREV) in T cells that are characterized by the presence of either FasL or granzyme B upon enrichment by density gradient centrifugation and are referred to as type 1 and type 2 LREV, respectively. Electron micrographs of the enriched organelles revealed apparent differences in size and electron density. Moreover, proteomic profiling not only confirmed the lysosomal character of both LREV species but also revealed striking differences in protein content with respect to cytotoxic effector proteins and in the association with cytoskeletal elements indicative of differential mechanisms of release (Lettau et al., 2015; Schmidt et al., 2011a, b). We had noted before that in PHA-stimulated T-cell blasts, also the 9 kDa form and the 15 kDa form of GNLY segregate to these different LREV (Schmidt et al., 2011a, 2009; Schmidt et al., 2009). Employing this well-established enrichment protocol, we thus searched for the presence of the two GNLY forms in individual lysosomal fractions of enriched organelles from MACS-sorted $CD4^+$ or $CD8^+$ T-cell blasts and zoledronate-stimulated ($V\delta2^+$) TCR $\gamma\delta^+$ T cells by Western blot analyses. As documented in Fig. 3, in all cases we observed a clear and almost exclusive segregation of the unprocessed 15 kDa form to type 1 LREV (present in the lighter fractions 2 or 3 of the gradients) whereas the short 9 kDa GNLY was markedly enriched in more dense fractions and especially in fraction 6 of the gradient containing type 2 LREV. Of note, we had defined type 1 LREV on the basis of the presence of FasL (see also Fig. 3) and of a decoration with actin-regulating cytoskeletal elements (Schmidt et al., 2011a, b). Morphologically, these type 1 LREV are intermediately electron-dense, heterogenous in size and separate in discontinuous iodixanol gradients from other vesicles such as mitochondria or dense granules. Importantly, electron-dense type 2 LREV store and transport PRF and Grzs and are thus considered to resemble conventional cytotoxic granules (Lettau et al., 2015; Schmidt et al., 2011a, b). The Western blotting results further indicate that the activation-dependent processing of GNLY to the 9 kDa form is a more prominent feature of TCR $\alpha\beta^+$ $CD8^+$ and TCR $\gamma\delta^+$ T cells than of TCR $\alpha\beta^+$ $CD4^+$ T cells.

In order to visualize and statistically prove that also in intact cells, the 9 kDa and 15 kDa GNLY segregate to distinct LREV, we employed imaging flow cytometry. We used activated and expanded TCR $\gamma\delta^+$ T cells and ($CD8^{+low}$) $CD56^+$ NK cells and stained for GrzA and CD107a as markers for conventional cytotoxic granules/type 2 LREV and with two different anti-GNLY reagents that allowed us to distinguish between the long and short form (Fig. 4). It had been previously shown for PFA-fixed samples that the monoclonal antibody RF10 exclusively binds to the full length 15 kDa variant since the targeted epitope is missing in the shorter 9 kDa variant. Immunoprecipitation and Western blot revealed that the used polyclonal antibody recognises both variants with a clear preference for the 9 kDa form. Interestingly, in PFA-fixed cells the polyclonal antibody almost exclusively detects the 9 kDa form which was already observed before (Clayberger et al., 2012; Dominovic et al., 2016). It was suggested that the 15 kDa molecule might adopt a conformation that masks epitopes that are also present in the 9 kDa form (Clayberger et al., 2012). The ImageStream analysis revealed a high percentage of GNLY-positive cells in both populations that were positive for both, the 9 kDa and the 15 kDa form. However, only the polyclonal antiserum (pc) stained GNLY in $CD107a^+$ and in $GrzA^+$ vesicles indicating that those selectively contain the processed 9 kDa form. The bright detail similarity feature statistically confirmed this notion (Fig. 5). The mean BDS score for 15 kDa GNLY/CD107a and 15 kDa GNLY/GrzA-double positivity was around 1 whereas the BDS score for the 9 kDa GNLY/CD107a and the 9 kDa GNLY/GrzA staining was in the range of 1.6 which resembles BDS scores observed for the colocalization of PRF and GrzB with CD107a in comparable experimental setups (Lettau et al., 2018). Notably, colocalization of GNLY with CD107a appeared even more pronounced employing the directly labelled anti-GNLY antibody clone DH2. It has been shown before, that this antibody recognizes a conformation-dependent epitope within the portion of GNLY that is also present in the 9 kDa form and ELISA experiments indicated that clone DH2 preferentially recognizes the 9 kDa variant (Hanson et al., 1999). Conclusively, 9 kDa GNLY, but not 15 kDa GNLY localizes to CD107a-decorated $GrzA^+$ granules.

We recently reported that type 1 and type 2 LREV display different requirements for mobilization and for degranulation. We have shown in comparable experimental setups, that FasL as a transmembrane component of type 1 LREV is mobilized by phorbol ester alone and thus in a non-classical calcium-independent degranulation process following PKC activation, whereas GrzB release and CD107a mobilization depend on the presence of the calcium ionophore ionomycin indicative of classical calcium-dependent degranulation. In this setting, the calcium chelator EGTA completely abrogated mobilization of GrzB and CD107a but did not modulate activation-induced translocation of pre-stored FasL molecules to the cell surface (Lettau et al., 2018). We now show that the two forms of GNLY follow exactly the proposed and expected routes for individual LREV. For this experiment, we stimulated and expanded TCR $\gamma\delta^+$ T cells expressing high levels of GNLY. After 14 days of expansion, we re-stimulated the cells with phorbol ester alone to activate only PKC or with phorbol ester and ionomycin to induce classical calcium-dependent degranulation. The result documented in Fig. 6 was very clear: Besides some constitutive release of 15 kDa GNLY into the culture supernatant PKC activation results in a further increase

of only the long GNLY form. In the presence of ionomycin the 9 kDa variant is deliberated in high amounts by classical calcium-dependent degranulation. As a further proof, this calcium-dependent release of 9 kDa GNLY is completely shut off in the presence of EGTA, whereas the PKC-induced release is still detectable. Of note, both FasL and 15 kDa GNLY follow the same requirements for release and co-fractionate upon density gradient centrifugation in fractions referred to as type 1 LREV. However, since it is yet unclear whether type 1 LREV constitute a heterogenous population of storage organelles it remains to be proven whether FasL and 15 kDa GNLY indeed employ the same individual effector vesicle entity for storage and mobilization.

Collectively, our present data strongly support several recent findings regarding GNLY biology. First, GNLY is differentially distributed in different subsets of T cells and NK cells. In T cells, GNLY expression goes in line with activation and maturation of LREV. In innate lymphocytes, such as NK cells and TCR $\gamma\delta^+$ T cells, constitutive GNLY expression appeared even higher than in classical $CD8^+$ TCR $\alpha\beta^+$ CTL. This is in agreement with recent findings by in-depth profiling of human T and NK cells for patterns of differentiation and cytotoxic-molecule abundance by mass cytometry (Bengsch et al., 2018) and also with the GNLY content analyses in decidual lymphocytes by Dominovic and colleagues (Dominovic et al., 2016). In the latter work, it was further demonstrated that fresh decidual lymphocytes display inferior cytotoxic activity, but after cell activation the cytotoxic potential increases due to an accumulation of 9 kDa GNLY in PRF- and CD107a-containing vesicles.

It has been shown that in the extracellular space, 15 kDa GNLY acts as an 'alarmin' and enhances immunologic reactions by recruiting and activating immunocompetent cells such as macrophages to the site of inflammation (Tewary et al., 2010) and major antimicrobial activity has been attributed to the processed 9 kDa variant which operates most efficiently when it is released together with PRF and GrzB (Balin et al., 2018). Accordingly, a selective induction of the release of the two GNLY forms could theoretically drive the immune response into an inflammatory or an effector direction. Here, the identification of surface receptors, additional factors and of associated signaling pathways that govern the fine-tuning of the cytotoxic response with respect to the differential release of effector molecules in different effector/target cell situations might help to shed light on the regulation of GNLY function in a physiological context.

5. Conclusion

The localization of the different forms of GNLY to individual LREV directly correlates with the signal requirements for degranulation and release of FasL or PRF and GrzB, respectively. Thus, the activation-induced release of 15 kDa GNLY serves as a further marker for calcium-independent non-classical degranulation whereas the release of 9 kDa GNLY indicates calcium-dependent classical degranulation. Since the two degranulation processes might be differentially triggered, a distinct activation of $GNLY^+$ effector cells might be employed to specifically modulate the onset of an inflammatory immune response by inducing the release of 15 kDa GNLY (and increased FasL expression) or to force target cell destruction and promote antimicrobial activity by initiating the release of 9 kDa GNLY together with PRF and GrzB.

Declarations of interest

None.

Acknowledgements

This work was supported by the German Research Foundation [grant number JA 610 7-1]; and the Medical Faculty of the University of Kiel. The authors thank Ina Martens for expert technical assistance. This work forms part of the MD Theses of Michelle Dietz and Katharina Dohmen.

Appendix A. Supplementary data

Supplementary material related to this article can be found, in the online version, at doi:https://doi.org/10.1016/j.molimm.2018.12.031.

References

Alter, G., Malenfant, J.M., Altfeld, M., 2004. CD107a as a functional marker for the identification of natural killer cell activity. J. Immunol. Methods 294, 15–22. https://doi.org/10.1016/j.jim.2004.08.008.

Al-Wasaby, S., de, M.D., Aporta, A., Naval, J., Conde, B., Martinez-Lostao, L., Anel, A., 2015. In vivo potential of recombinant granulysin against human tumors. Oncoimmunology 4, e1036213. https://doi.org/10.1080/2162402X.2015.1036213. 1036213 [pii].

Anderson, D.H., Sawaya, M.R., Cascio, D., Ernst, W., Modlin, R., Krensky, A., Eisenberg, D., 2003. Granulysin crystal structure and a structure-derived lytic mechanism. J. Mol. Biol. 325, 355–365 S0022283602012342 [pii].

Balin, S.J., Pellegrini, M., Klechevsky, E., Won, S.T., Weiss, D.I., Choi, A.W., Hakimian, J., Lu, J., Ochoa, M.T., Bloom, B.R., Lanier, L.L., Stenger, S., Modlin, R.L., 2018. Human antimicrobial cytotoxic T lymphocytes, defined by NK receptors and antimicrobial proteins, kill intracellular bacteria. Sci. Immunol. 3https://doi.org/10.1126/sciimmunol.aat7668. 3/26/eaat7668 [pii].

Bengsch, B., Ohtani, T., Herati, R.S., Bovenschen, N., Chang, K.M., Wherry, E.J., 2018. Deep immune profiling by mass cytometry links human T and NK cell differentiation and cytotoxic molecule expression patterns. J. Immunol. Methods 453, 3–10. https://doi.org/10.1016/j.jim.2017.03.009. S0022-1759(17)30132-1 [pii].

Betts, M.R., Brenchley, J.M., Price, D.A., De Rosa, S.C., Douek, D.C., Roederer, M., Koup, R.A., 2003. Sensitive and viable identification of antigen-specific CD8+ T cells by a flow cytometric assay for degranulation. J. Immunol. Methods 281, 65–78.

Che, Y., Lu, Y., Zha, X., Huang, H., Yang, P., Ma, L., Xu, X., 2016. Higher efficiency soluble prokaryotic expression, purification, and structural analysis of antimicrobial peptide G13. Protein Expr. Purif. 119, 45–50. https://doi.org/10.1016/j.pep.2015.11.006.

Chung, W.H., Hung, S.I., Yang, J.Y., Su, S.C., Huang, S.P., Wei, C.Y., Chin, S.W., Chiou, C.C., Chu, S.C., Ho, H.C., Yang, C.H., Lu, C.F., Wu, J.Y., Liao, Y.D., Chen, Y.T., 2008. Granulysin is a key mediator for disseminated keratinocyte death in Stevens-Johnson syndrome and toxic epidermal necrolysis. Nat. Med. 14, 1343–1350. https://doi.org/10.1038/nm.1884. nm.1884 [pii].

Clayberger, C., Finn, M.W., Wang, T., Saini, R., Wilson, C., Barr, V.A., Sabatino, M., Castiello, L., Stroncek, D., Krensky, A.M., 2012. 15 kDa granulysin causes differentiation of monocytes to dendritic cells but lacks cytotoxic activity. J. Immunol. 188, 6119–6126. https://doi.org/10.4049/jimmunol.1200570. jimmunol.1200570 [pii].

Deng, A., Chen, S., Li, Q., Lyu, S.C., Clayberger, C., Krensky, A.M., 2005. Granulysin, a cytolytic molecule, is also a chemoattractant and proinflammatory activator. J. Immunol. 174, 5243–5248 174/9/5243 [pii].

Dominovic, M., Laskarin, G., Glavan, G.L., Haller, H., Rukavina, D., 2016. Colocalization of granulysin protein forms with perforin and LAMP-1 in decidual lymphocytes during early pregnancy. Am. J. Reprod. Immunol. 75, 619–630. https://doi.org/10.1111/aji.12503.

Dotiwala, F., Mulik, S., Polidoro, R.B., Ansara, J.A., Burleigh, B.A., Walch, M., Gazzinelli, R.T., Lieberman, J., 2016. Killer lymphocytes use granulysin, perforin and granzymes to kill intracellular parasites. Nat. Med. 22, 210–216. https://doi.org/10.1038/nm.4023. nm.4023 [pii].

Hanson, D.A., Kaspar, A.A., Poulain, F.R., Krensky, A.M., 1999. Biosynthesis of granulysin, a novel cytolytic molecule. Mol. Immunol. 36, 413–422 S0161589099000632 [pii].

Hecht, O., Van Nuland, N.A., Schleinkofer, K., Dingley, A.J., Bruhn, H., Leippe, M., Grötzinger, J., 2004. Solution structure of the pore-forming protein of *Entamoeba histolytica*. J. Biol. Chem. 279, 17834–17841. https://doi.org/10.1074/jbc.M312978200. M312978200 [pii].

Kita, Y., Hashimoto, S., Nakajima, T., Nakatani, H., Nishimatsu, S., Nishida, Y., Kanamaru, N., Kaneda, Y., Takamori, Y., McMurray, D., Tan, E.V., Cang, M.L., Saunderson, P., Dela Cruz, E.C., Okada, M., 2013. Novel therapeutic vaccines [(HSP65 + IL-12)DNA-, granulysin- and Ksp37-vaccine] against tuberculosis and synergistic effects in the combination with chemotherapy. Hum. Vaccine Immunother. 9, 526–533 23230 [pii].

Kolter, T., Winau, F., Schaible, U.E., Leippe, M., Sandhoff, K., 2005. Lipid-binding proteins in membrane digestion, antigen presentation, and antimicrobial defense. J. Biol. Chem. 280, 41125–41128. https://doi.org/10.1074/jbc.R500015200. R500015200 [pii].

Krensky, A.M., Clayberger, C., 2009. Biology and clinical relevance of granulysin. Tissue Antigens 73, 193–198. https://doi.org/10.1111/j.1399-0039.2008.01218.x.

Lettau, M., Kabelitz, D., Janssen, O., 2015. Lysosome-related effector vesicles in T lymphocytes and NK cells. Scand. J. Immunol. 82, 235–243. https://doi.org/10.1111/sji.12337.

Lettau, M., Armbrust, F., Dohmen, K., Drews, L., Poch, T., Dietz, M., Kabelitz, D., Janssen, O., 2018. Mechanistic peculiarities of activation-induced mobilization of cytotoxic effector proteins in human T cells. Int. Immunol. 30, 215–228. https://doi.org/10.1093/intimm/dxy007.

Liepinsh, E., Andersson, M., Ruysschaert, J.M., Otting, G., 1997. Saposin fold revealed by the NMR structure of NK-lysin. Nat. Struct. Biol. 4, 793–795.

Martinez-Lostao, L., de, M.D., Al-Wasaby, S., Gallego-Lleyda, A., Anel, A., 2015. Death ligands and granulysin: mechanisms of tumor cell death induction and therapeutic opportunities. Immunotherapy 7https://doi.org/10.2217/imt.15.56. 883-2.

Nagasawa, M., Isoda, T., Itoh, S., Kajiwara, M., Morio, T., Shimizu, N., Ogawa, K., Nagata, K., Nakamura, M., Mizutani, S., 2006. Analysis of serum granulysin in patients with hematopoietic stem-cell transplantation: its usefulness as a marker of graft-versus-host reaction. Am. J. Hematol. 81, 340–348. https://doi.org/10.1002/ajh.20570.

Ogawa, K., Takamori, Y., Suzuki, K., Nagasawa, M., Takano, S., Kasahara, Y., Nakamura, Y., Kondo, S., Sugamura, K., Nakamura, M., Nagata, K., 2003. Granulysin in human serum as a marker of cell-mediated immunity. Eur. J. Immunol. 33, 1925–1933. https://doi.org/10.1002/eji.200323977.

Pena, S.V., Hanson, D.A., Carr, B.A., Goralski, T.J., Krensky, A.M., 1997. Processing, subcellular localization, and function of 519 (granulysin), a human late T cell activation molecule with homology to small, lytic, granule proteins. J. Immunol. 158, 2680–2688.

Sarwal, M.M., Jani, A., Chang, S., Huie, P., Wang, Z., Salvatierra Jr., O., Clayberger, C., Sibley, R., Krensky, A.M., Pavlakis, M., 2001. Granulysin expression is a marker for acute rejection and steroid resistance in human renal transplantation. Hum. Immunol. 62, 21–31.

Schmidt, H., Gelhaus, C., Lucius, R., Nebendahl, M., Leippe, M., Janssen, O., 2009. Enrichment and analysis of secretory lysosomes from lymphocyte populations. BMC Immunol. 10. https://doi.org/10.1186/1471-2172-10-41.

Schmidt, H., Gelhaus, C., Nebendahl, M., Lettau, M., Lucius, R., Leippe, M., Kabelitz, D., Janssen, O., 2011a. Effector granules in human T lymphocytes: proteomic evidence for two distinct species of cytotoxic effector vesicles. J. Proteome Res. 10, 1603–1620. https://doi.org/10.1021/pr100967v.

Schmidt, H., Gelhaus, C., Nebendahl, M., Lettau, M., Lucius, R., Leippe, M., Kabelitz, D., Janssen, O., 2011b. Effector granules in human T lymphocytes: the luminal proteome of secretory lysosomes from human T cells. Cell Commun. Signal 9. https://doi.org/10.1186/1478-811X-9-4.

Stenger, S., Hanson, D.A., Teitelbaum, R., Dewan, P., Niazi, K.R., Froelich, C.J., Ganz, T., Thoma-Uszynski, S., Melian, A., Bogdan, C., Porcelli, S.A., Bloom, B.R., Krensky, A.M., Modlin, R.L., 1998. An antimicrobial activity of cytolytic T cells mediated by granulysin. Science 282, 121–125.

Tewary, P., Yang, D., de la Rosa, G., Li, Y., Finn, M.W., Krensky, A.M., Clayberger, C., Oppenheim, J.J., 2010. Granulysin activates antigen-presenting cells through TLR4 and acts as an immune alarmin. Blood 116, 3465–3474. https://doi.org/10.1182/blood-2010-03-273953.

Walch, M., Dotiwala, F., Mulik, S., Thiery, J., Kirchhausen, T., Clayberger, C., Krensky, A.M., Martinvalet, D., Lieberman, J., 2014. Cytotoxic cells kill intracellular bacteria through granulysin-mediated delivery of granzymes. Cell 157, 1309–1323. https://doi.org/10.1016/j.cell.2014.03.062.

Wei, H.M., Lin, L.C., Wang, C.F., Lee, Y.J., Chen, Y.T., Liao, Y.D., 2016. Antimicrobial properties of an immunomodulator - 15 kDa human granulysin. PLoS One 11, e0156321. https://doi.org/10.1371/journal.pone.0156321.